Dynamic contrast enhanced – MRI efficiency in detecting embolization-induced perfusion defects in a rabbit model of critical-limb-ischemia

Gabriel Ifergan, Gwennhael Autret, Costantino del Giudice, Augustin Lecler, Adrien Lalot, Camille Marijon, Amaury Casanova, Mailyn Perez-Liva, Valérie Bellamy, Patrick Bruneval, et al.

Version of Record: https://www.sciencedirect.com/science/article/pii/S0730725X22000017
Manuscript_e812c8a09463c52019bff1d2a120a50d

Dynamic Contrast Enhanced - MRI efficiency in detecting embolization-induced perfusion defects in a rabbit model of critical-limb-ischemia.

Ifergan Gabriel [a], Autret Gwennhael [a], Del Giudice Costantino [a,b], Lecler Augustin [a,c], Lalot Adrien[a], Marijon Camille [a], Casanova Amaury [a], Perez-Liva Mailyn [a], Bellamy Valérie [a], Bruneval Patrick [a,b], Clement Olivier [a,b], Sapoval Marc [a,b], Menasché Philippe [a,b], Balvay Daniel [a].

a – Regenerative Therapies for Cardiac and Vascular Diseases / In vivo Imaging Research / Integrative Epidemiology of Cardiovascular diseases, Université de PARIS, PARCC U970, INSERM
b – Interventional Radiology / Radiology / Anatomy Pathology /horacic and cardiovascular surgery, Hôpital Européen Georges Pompidou, APHP
c – Fondation Ophtalmologique Adolphe de Rothschild

Research Article: 5332 words

Keywords: perfusion, DCE-MRI, CLI, heterogeneity, ischemia, hyperemia, rabbit

Ifergan Gabriel: gabriel_ifergan@hotmail.fr

Autret Gwennhael: gwennhael.autret@inserm.fr

Del Giudice Costantino: costantino.del-giudice@aphp.fr

Lecler Augustin: alecler@for.paris

Lalot Adrien: adrienlalot@hotmail.fr

Marijon Camille: c.marijon15@imperial.ac.uk

Casanova Amaury: amaury.casanova@yahoo.fr

Perez-Liva Mailyn: mailyn.perez-liva@inserm.fr

Bellamy Valérie: valerie.bellamy@inserm.fr

Bruneval Patrick: patrick.bruneval@inserm.fr

Clement Olivier: olivier.clement@aphp.fr

Sapoval Marc: marc.sapoval2@aphp.fr

Menasché Philippe: philippe.menasche@aphp.fr

Balvay Daniel: daniel.balvay@inserm.fr

Corresponding author: daniel.balvay@inserm.fr

Daniel Balvay, PARCC-HEGP (Eq2)

56 rue Leblanc, 75015 PARIS, FRANCE

Tel: +33 1 53 98 8038 Fax: +33 1 53 98 79 52

Funding. This study was supported by funds from the Fondation Coeur et Artères (FCA 15T3).

Declarations of interest: none

ABSTRACT

Critical limb ischemia (CLI) is a severe disease which affects about 2 million people in the US. Its prevalence is assessed at 800 / 100000 population. However, no reliable tools are currently available to assess perfusion defects at the muscle tissue level. DCE-MRI is a technique that holds the potential to be effective in achieving this goal. However, preclinical studies performed with DCE-MRI have indicated low sensitivity assessing perfusion at resting state. To improve these previous results, in this work we propose new methodologies for data acquisition and analysis and we also revisit the biological model used for evaluation.

Eleven rabbits underwent embolization of a lower limb. They were imaged at day 7 after embolization using DCE-MRI, performed on a 4.7T small imaging device. Among them, n=4 rabbits were used for MRI sequence optimization and n=7 for data analysis. Normalized Areas under the curve (AUCn), and kinetic parameters such as K_{trans} and *Vd* resulting from the Tofts-Kety modeling (KTM) were calculated on the embolized and contralateral limbs. Average and heterogeneity features, consisting on standard-deviation and quantiles, were calculated on muscle groups and whole limbs. The Wilcoxon and Fisher-tests were performed to compare embolized and contralateral regions of interests. The Wilcoxon test was also used to compare features of parametric maps. Quantiles of 5 and 95% in the contralateral side were used to define low and high outliers. A *P*-value < 0.05 was considered statistically significant.

Average features were inefficient to identify injured muscles, in agreement with the low sensitivity of the technique previously reported by the literature. However, these findings were dramatically improved by the use of additional heterogeneity features (97% of total accuracy for group muscles, P<0.01 and 100% of total accuracy for the total limbs). The mapping analysis and automatic outlier detection quantification improvement was explained by the presence of local hyperemia that impair the average calculations. The analysis with KTM did not provide any additional information compared to AUCn.

The DCE technique can be effective in detecting embolization-induced disorders of limb muscles in a CLI model when heterogeneity is taken into account in the data processing, even without vascular stimulation. The simultaneous presence of areas of ischemia and hyperemia appeared as a signature of the injured limbs. These areas seem to reflect the simultaneous presence of infarcted areas and viable peripheral areas, characterized by a vascular response that is visible in DCE.

Keywords: perfusion, DCE-MRI, CLI, heterogeneity, ischemia, hyperemia, rabbit

1 INTRODUCTION

Critical limb ischemia (CLI) is the end-stage of peripheral arterial disease (PAD) caused by a chronic low tissue perfusion of extremities. CLI is characterized by resting pain and foot trophic disorders [1–3] with a high morbidity and mortality [4,5]. Digital subtraction angiography is considered the gold standard to characterize associated arterial disease to plan surgical or endovascular interventions [6]. However, even when angiography can detect macrovascular lesions, it prevents the detailed evaluation of the resulting perfusion defects in the downstream muscles. In particular, it is difficult to assess the extent of infarcted and viable muscle territories. This challenge becomes more important after a complex remodeling involving complex collateralization [7] and when the pathology affects small vessels as in diabetic patients [8]. Several approaches are used in clinical practice to evaluate foot perfusion, such the ankle brachial index, molecular imaging, and transcutaneous oxygen evaluation. Yet, they present low sensitivity [9–11].

Dynamic contrast enhanced (DCE) imaging provides a non-invasive assessment of microcirculation [12] and is widely performed in oncological research [13]. The main advantages of DCE-MRI are the limitation of radiation doses and the ability to combine perfusion with T1 and T2 sequences used for characterizing morphology and inflammation with a good spatial resolution [14]. However, so far, preclinical DCE-MRI results have not been very encouraging on conventional CLI models, particularly at rest [15]. Once the acute phase of the vascular pathology is overcome, the sensitivity of the DCE drops to the point of becoming ineffective

to detect ischemia. More convincing results were obtained under stress, i.e., with the help of vascular stimulation by chemical means, effort, or ischemia-reperfusion challenges [16,17].

In this study we tried to understand and improve the poor results obtained in DCE-MRI at rest. The low detection efficiency may have several causes: (1) an overly resilient biological model inducing rapid vascular restoration; (2) a low signal-to-noise ratio, potentially combined with overly unstable analysis tools; and (3) an analysis method not finding the right piece of information in the data. Here we sought to minimize issues associated with data acquisition and biological model, and focused on revisiting the standard data processing methodology to adapt it to the analysis of heterogeneous phenomena.

2 MATERIALS AND METHODS

2.1 ANIMAL PROTOCOL

The animal experimentation was approved by the Ethical Committee of the local institutional Animal Care and Use Committee (project n° 16003). All procedures were performed under intramuscular anesthesia with a mixture of ketamine (50 mg/kg) and xylazine (5 mg/kg). Animal ventilation was carried out with a laryngeal mask, and body temperature was maintained at 37 °C**.** Preventive analgesia was provided to rabbit with a 3-day patch of fentanyl 12 µg/h. Eleven New Zealand white male rabbits weighting 4.5-5.5 kg were included: four for the optimization of the DCE sequence and seven for the perfusion analysis. Imaging was performed on day 7, corresponding to a subacute phase, to avoid acute inflammation induced by embolization and allow intervals between anesthesia.

2.2 SURGICAL PROCEDURE

CLI model has been previously described elsewhere [18]. It is an embolization model comparable to the one used by Hur [8]. In short, the model was obtained by percutaneous embolization from the superficial femoral artery (SFA) and its branches using 300–500 µm calibrated particles to obtain a distal ischemia until the distal capillary vessels of the same range (Embosphere, Merit Medical UT, USA). The procedure, angiography-guided, was performed through a total percutaneous approach through the auricular artery without need of surgical incision. The procedure was performed unilaterally, resulting in an embolized and a contralateral limb.

2.3 MR IMAGING

MRI was performed with a dedicated small animal 4.7 T MRI system (Biospec 47/40 USR, Bruker, Billerica, Massachussets, USA) using a quadrature transmit/receive body coil with a 20 cm inner diameter. Rabbits were imaged in natural sitting position (bun loaf). An auricular vein catheter was inserted for animal perfusion of saline solution and injection of contrast agent (Gadolinium, gadoterate meglumine, Dotarem®, Guerbet, Aulnay-sous-Bois, France, 500 mmol Gd/L).

A Turbo RARE T2-w sequence was performed on calf muscle groups, before injection, with special attention on localization to improve symmetry between limbs.

The parameters of the FLASH DCE sequence are shown in table 1. In this multi-2D sequence, where TRs cannot be as low as in 3D sequences, a high flip angle was chosen to avoid signal saturation for high contrast agent (CA) concentrations. However, non-linearity effects between MRI signal and concentration may still occur for higher CA concentrations. To limit assessment errors, or the use of correction techniques (such as T1 mapping or tube

calibration), which may not be mastered outside of specialized DCE centers, the bolus was split into two boluses [19].

After a preliminary experiment including four rabbits to adjust acquisition settings, a first bolus of diluted CA solution (1/10) was injected one minute after the beginning of the DCE sequence, flushed by 3 mL of saline; then, one minute later, a second bolus of 1 mL of pure CA solution flushed by 2 mL of saline was delivered. Therefore, 1.3 mL of Gd was injected corresponding with 0.29 mL of Dota/kg for rabbits (1.5 x clinical dose). The time resolution/duration were: 3.15s/12 min, corresponding to 230 time points. High baseline and total acquisition duration were chosen to minimize errors due to low SNRs.

After the DCE sequence, a Turbo RARE T1-w sequence was performed. For more details, see Table 1.

2.4 DCE-MRI Analysis

Regions of interests were delineated manually in both iliac arteries. The artery with the maximum signal was used to define the unique arterial input functions (AIF) of the rabbit (minimal partial volume effect expected). Then, muscle groups were delineated both in embolized and contralateral sides. Three calf muscle groups were drawn: anterior (ANT), deep (DEEP) and posterior (POST). These regions of interest (ROIs) were drawn thanks to the corresponding T2-w sequence where muscles were visible. Additionally, on each side, a global region (TOT) including all the limb in the slice was delineated.

DCE data correspond to MRI intensities acquired for consecutive time points. This results in a time intensity curve (TIC) for each pixel. Contrast enhancements were evaluated from TIC by subtracting the TIC values from the average of the TIC before the CA injection (baseline). A spatial average was also performed in AIFs and each muscle region (ANT, DEEP and POST) for

each time, resulting in averaged TICs (ROIs analysis). The contrast enhancement was also evaluated pixel by pixel to assess perfusion heterogeneity (map analysis). Normalized area under the curves (AUCn) was calculated both for ROIs and maps analysis. The area under the curve (AUC) was calculated by evaluating the integral of the muscular enhancement over time. This value was then normalized by the AUC of the AIF. The result was AUCn. Not-normalized AUC were also calculated for comparison with AUCn, and consider a context where AIFs are lacking [20]. AUCn and AUC were calculated over the entire duration of the acquisitions.

For the ROIs Analysis, AUCn was completed by a compartmental analysis. The one-compartment Tofts-Kety (TK) pharmacokinetic model was used to assess the K_{trans} and V_d parameters[21]. K_{trans} corresponds to the tissue filling rate while V_d, the volume of distribution, represents the accumulation capacity of the contrast agent into the muscle. The TK model is widely used in oncology. It is commonly preferred to more complex models to improve the robustness of analysis [22]. This robustness is particularly sought in our analysis, as lower SNRs are expected in resting muscles than in tumors that are commonly characterized by intense angiogenesis. The TK model parameters were calculated using a homemade software developed in Matlab® (Mathwork, Natick) [23], based on a nonlinear least-squares method with the following initialisation: K_{trans} = 240 ml/min/100ml and V_d = 10%. Moreover, AUCn was roughly approximated by calculating a simple difference in the pixels before and after injection. The resulting parameter, ΔS, was calculated by subtracting the average of the last ten TIC values from the average of their first ten values.

AUCn, K_{trans}, *Vd* and ΔS were correlated. Then, the parameters were compared, “Embolized” vs. “Contralateral,” to test the ability of the DCE to detect embolized muscles. In line with

the literature, a nonparametric Wilcoxon test was performed to control the hypothesis of a global decrease of perfusion in the embolized muscles (Hyp 1). This conventional test was supplemented by a Fisher test, to control the hypothesis of an increase in the variability (variance) of perfusion parameters between muscles in the embolized muscles (Hyp 2).

The map analysis was conducted to clarify the results of the tests performed on averages, on the ANT, DEEP, POST regions. Features corresponding to central tendencies (average, median, mode) into each region were calculated to specify the previous result for Hyp 1. Features of dispersion (standard deviation, median absolute deviation (MAD), range) were calculated into each region to specify the previous result for Hyp 2. Moreover, five outlier features were calculated to identify the presence of abnormally low or high perfusion levels in the embolized muscles. The first two features were the 5% and 95% percentiles (P5 and P95) calculated into each muscle map. The last three features consider the percentiles (P5C and P95C) calculated on the pixels of all the contralateral limbs (TOT). These thresholds defined hypo-perfused pixels (HYPO <P5C), hyper-perfused pixels (HYPER> P95C) and normally perfused pixels (P5C ≤ ISO ≤ P95C), all versus the contralateral population. The three corresponding features were the low, high, and total outlier fractions (LOF, HOF, TOF), corresponding respectively to the percentage of HYPO, HYPER and HYPO + HYPER pixels into the AUCn maps. All map features were compared between embolized and contralateral muscles, using the Wilcoxon tests. For comparison, the features were also calculated from the non-normalized AUC maps.

Furthermore, HYPO, ISO and HYPER pixels were drawn from TOT maps, resulting in “detection maps” to assess graphically the position and extent of the HYPO and HYPER

perfusion defects. Detection maps were generated from AUCn maps and alternatively from AUCn-180 calculated only during the first pass (180s post-bolus).

All calculations were performed in Matlab®.

2.5 HISTOLOGIC ANALYSIS

Histology was performed to confirm the severity of the animal model. On Day 14, a date commonly used to identify necrosis and tissue remodeling in muscles, animals were sacrificed by intravenous injection of potassium chloride under anesthesia. The gastrocnemius muscles from both limbs of five rabbits were removed, fixed in 10% formalin and embedded in paraffin. Five micrometers sections were stained with hematoxylin eosin saffron.

2.6 STATISTICAL ANALYSIS

Two types of statistical tests were used. Wilcoxon tests were performed to compare median values between groups ($P < 0.05$ was considered the threshold of significance). Variances were compared by using the Fisher test ($P < 0.05$ was also considered the threshold of significance). $P < 0.01$ as considered highly significant, while $P < 0.05$ was considered moderately significant.

3 RESULTS

3.1 CLI MODEL

3.1.1 CLINICAL OBSERVATIONS

The success of the angiography-guided embolization of the right superficial femoral artery was demonstrated by blood flow interruption, visible in the angiography-guided procedure. After this, all animals developed a painful right limb ischemia from Day 2. Five of them

developed severe ischemia with ischemic necrosis of extremities and calf ulceration. No signs of ischemia were observed in the contralateral limbs.

3.1.2 Detection of Inflammatory Disorders

The severity of the model was confirmed by T1 and T2 MRI imaging and histology. Combined T1-w post-injection and T2-w images (n=7) enabled the visualization of morphological and pathological patterns (Fig. 1). In embolized limbs, all T2-w images presented muscle groups with hypersignal and qualitatively increased volumes. Images highlighted inflammatory edema and muscular suffering. In contralateral limbs, all T1-w images showed hypersignal in aponeurosis and thigh muscles with a “featherlike” pattern consistent with tendinitis and muscular tears due to overuse compensatory injuries. A rabbit with a particularly severe contralateral inflammation was excluded from the analysis. Histologic data (n=5) indicated the presence of inflammation (3/5) with macrophages, muscle cells atrophy (2/5) and fibrosis (3/5) associated with remodeling in the embolized gastrocnemius muscles. The contralateral gastrocnemius muscles remained normal.

3.2 DCE IMAGING

3.2.1 Signal observations

AIF was successfully evaluated for each rabbit. Globally, the signal was slightly higher in iliac arteries from embolized sides, indicating a possible slight arterial vasodilatation. The contrast enhancement in muscles groups confirmed both acceptable SNR and clear differences between embolized and contralateral sides, as illustrated Fig. 2 for one rabbit. In this figure, the contralateral muscle kinetics are close together. This homogeneity was globally observed for all rabbits. Conversely, kinetics of the embolized muscles were mainly heterogeneous, often with either hypo- or hyper-perfusion patterns, as shown in Fig. 2.

3.2.2 ROI ANALYSIS

AUCn, *Ktans* and V_d were calculated in each Roi (muscle groups) and summarized in Fig. 3. The Wilcoxon-tests were negative for AUCn and V_d, and positive for K_{trans}. However, as shown in Fig. 3, the difference observed for K_{trans} was related to high K_{trans} values on the embolized side. It was contrary to what would be expected in the case of ischemia. Thus, the hypothesis Hyp 1 was invalidated. We did not detect any reduction in global perfusion corresponding to generalized ischemia. The Fisher-Tests were highly significant for all the parameters. Thus, the Hyp 2 hypothesis was confirmed. Embolization induced a high variability of the muscle responses as shown by AUCn, K_{trans} and V_d. The increased variability of perfusion between muscles was associated with both abnormally low or high perfusion in embolized muscles compared to contralateral ones. Quantitatively, almost 90% of the AUCn values in the embolized muscles were below or above the values found in the contralateral muscles.

The correlation coefficient calculated between both the TK parameters was $r^2 = 0.77$ for values of $V_d > 1\%$, indicating a high redundancy. For $V_d < 1\%$, we found no correlation, the K_{trans} values appeared random (supplementary Fig. S1), due to very low SNR in ischemic tissues. The correlation coefficients found between AUCn and V_d, and between AUCn and ΔS, were higher than 0.98. This indicated a fair equivalence between the three approaches. No differences were found between anterior, deep and posterior muscle groups. The correlation between AUCn and AUC was poor $r^2 = 0.35$. The impact of this difference was assessed in the maps analysis.

3.2.3 MAPS ANALYSIS

AUCn maps were provided on each side of the whole limb (TOT). Features of central tendency (average, median and mode) were plotted in Fig. 4.A. In line with the literature,

neither the averages nor the medians indicated a reduction of the global perfusion in the embolized limbs (P> 0.05). However, the Wilcoxon-Test indicated a difference between modes (P <0.05). Near-zero AUCn modes can be observed in the figure, in almost all embolized limbs, indicating the presence of substantial ischemic areas which were not visible with averages. A histogram analysis provides insight into the discordance between modes and means (Fig. S2). In the embolized limbs, all dispersion features showed an increase in spatial variability (P <0.01), demonstrating either noise or high spatial heterogeneity of the AUCn maps on the embolized sides. All outsider features indicated an increase of extreme perfusion values in embolized limbs, including both low and high perfusion values (P <0.01, Fig 4.B-C). Furthermore, the ranges of values of the perfusion features are disjointed between the embolized group and the contralateral group (except for one rabbit for one feature). It is therefore possible to classify the embolized limbs without any error by a simple threshold on one of these features. The difference was particularly noticeable for the total outlier fraction, with values close to 10% on the contralateral side, whereas TOF obtained on the embolized side were never less than 40%.

The spatial distributions of perfusion defects (detection maps) displaying low and high outlier pixels were generated (Fig. 5) for the 6 rabbits of the DCE study, and for the rabbit excluded due to a major contralateral inflammation (star in Fig.5). Most of the maps on the embolized sides showed strong spatial heterogeneity, including both distinct areas of hypo- and hyper-perfusion. The apparent noise in the maps was low. Three perfusion patterns were identified in the embolized limbs: (1) hypoperfusion of most muscle groups, supplemented by peripheral hyper-perfusion (Fig 5.B, E, G); (2) hypo-perfusion of the anterior muscles with hyperperfused posterior muscles and peripheral hyper-perfusion (Fig 5.C, F); (3) hyper-perfusion in the limb with focal hypoperfusion in each muscle group (Fig 5.A, D). Conversely,

contralateral limbs had a more homogeneous perfusion, except for the excluded rabbit (5% low and 5% high false positive outliers expected by definition).

AUCn maps were provided on each side of the ANT, DEEP and POST muscles and a decision tree was performed to classify embolized versus contralateral muscles, using only the mean and standard deviation features. As observed in Fig. 6, only one muscle was misclassified (97% total accuracy). Two trends can be considered for the embolized muscles: type 1: almost zero AUCn values on average with a moderate dispersion (ischemia confirmed in this subgroup), and type 2: average AUCn values comparable with contralateral, but higher standard deviations (revealing both the presence of hypo- and hyper-vascularized areas, in line with Hyp 2).

Statistical tests performed on mapping features did not change substantially with not-normalized AUCs (Fig. S3). Conclusions concerning averages and medians were not changed while the mode decreased, and all features of heterogeneity indicated differences between groups. Levels of significances were equivalent for most of the features. However, more overlaps were observed between embolized and control groups.

For AUCn-180, no changes were observed in the statistical tests calculated versus AUC (Fig. S4). However, detection maps performed on AUCn-180 were slightly noisier than the maps produced from the AUCn.

4 DISCUSSION

4.1 IMPROVED DETECTION

Critical limb ischemia commonly results from a single or multiple stenosis or occlusions induced by atherosclerosis. DCE imaging should be one of the most suitable imaging modalities to evaluate the consequences of these arterial pathologies on muscle microcirculation[6]. However, previous preclinical studies performed on CLI models did not confirm this hypothesis [15,24]. These results can be interpreted as follows. (1) DCE is not effective technically in assessing perfusion defects in muscles at rest. (2) The conventional model does not correspond to a true CLI model, due to rapid collateralization. (3) Conventional analysis misses the critical information contained in the DCE data. In our study we have sought to minimize the issues associated with the first two interpretations, to explore the analysis issues. The MRI sequence and CA injection were optimized and a biological model generating multiple occlusions was chosen to reduce the risks of collateralization. Then we looked for several analysis techniques allowing improvement in injured muscles detection.

Our results support that poor detection results found in the literature at rest can be explained only by concerns with the conventional average analysis. The average processing was blinded even for embolized limbs with a mean ischemic surface around 40% (see LOFs in Fig. 5). An efficient analysis was available but required *an additional feature of perfusion heterogeneity* (dispersion or outliers). These features were highly informative making that *almost each muscle group (ANT, DEEP, POST) and limb (TOT) could be identified individually* (non-overlapping distributions, classifier output). Furthermore, the outlier analysis showed that *limbs were characterized by both high ischemic areas (HYPO) and high hyperemic areas (HYPER).* Both were well delimited in space. Muscle embolization was therefore clearly detectable but only when considering that embolization can induce hyperemia next to ischemia.

4.2 SCALE ANALYSIS

The results of this study were performed at several spatial scales, from the whole limbs to pixel sets. The analysis at the whole limb scale (Fig.4) indicates that every embolized limbs showed a perfusion heterogeneity which was not visible in any control limb. It states that this heterogeneity was related to both hypo- and hyper-perfused pixels. The inter-muscle group (MG) analysis, (Fig. 3), showed a strong variability between the mean perfusion of the pathological MGs. This increase in variability was statistically demonstrated, based on all MGs. More interesting from a diagnostic point of view, nearly 90% of pathological MGs were either of ischemic or hyperemic type. This result indicates that the perfusion levels were spatially stable, at the MG scale. The analysis at the lower intra-muscle group scale (Fig. 6), indicates that a local mapping analysis enabled to detect each pathological MG individually but one. These maps indicated either global homogeneous ischemia or high perfusion heterogeneity, often associated with an increase in average perfusion. The analysis at the pixel scale (Fig. 5) was more qualitative. The parametric maps, in particular the detection maps, show well-structured spatial locations and extensions of hypo and hyper perfused zones. These maps enable identification of pathological zones from few pixels to almost the entire limb. This suggests that the mapping method could be considered to analyze lesions of various sizes, including smaller lesions than those generated by our model

4.3 INTERPRETATION

High AUCn values confirmed the presence of hyperemic areas post embolization. This hyperemia corresponds probably to a reaction of the vascular system against ischemia. This reactivity may have a role for the diagnosis. Moreover, it was demonstrated here that ignoring this phenomenon has a major detrimental effect for the ischemic detection.

Compensation effects between Hyper and Hypo regions prevents any detection with the averaging calculations. Paradoxical results obtained on the conventional ischemia model in previous studies can be explained by this phenomenon. Indeed, no average decrease in perfusion has been found in large regions except in a very early-stage post injury (Day 0+) [15,24,25]. The masking effect of the reactive hyperemia explains both the apparent recovery found in DCE after Day 0+, that is contradicted by independent measurements, and detection of ischemia at Day 0+, when the vascular response has not had time to develop.

Perfusion heterogeneity including hyperemia has already been reported in several chronic diseases in patients. For example, by Murray and al. in chronic rheumatic diseases evaluated by laser Doppler imaging [31]. Particularly related with PAD, Hur and al. [8] studied feet of patient suffering from PAD with DCE-CT. In their paper, parametric maps indicated a clear heterogeneity with frequent “bandlike hyperperfusion” in dermis. Thus, to consider heterogeneity could be relevant as well in a clinical context.

The presence of such heterogeneity is not particularly surprising [32]. Many mechanisms of vascular restoration come into action [32] in case of homeostasis disorders induced by embolization, such as fibrosis, angiogenesis [33], blood-organ-barrier changes [34], at the microcirculatory scale, and artegiogenesis [35,36]. These phenomena, which depend on several regulatory pathways, work in synergy to limit ischemic damages. Angiogenesis is notably activated at the sites of ischemic regions, via HIF and VEGF, whereas arteriogenesis - or collateralization - is rather activated in the territories next to the ischemia, via VCAM, which is promoted by an increase in shear stress induced by the rerouting of arterial flow towards the non-occluded arteries and arterioles. The distribution of the perfusion observations is therefore expected to be not uniform.

4.4 BIOLOGICAL MODEL.

The conventional rodent model underwent a unilateral arterial resection [26]. The biological model of emboli selected here could be considered as an improved alternative to this model which limits post-surgical inflammation, local fibrosis and collateralization. The model of emboli enables control of severity induced by a more spread occlusion. Rodents of the conventional model were replaced by rabbits to allow endovascular induction with an interventional radiology equipment. Other animal models have been previously proposed to approach more chronical patient pathologies to mimic evolutionary injuries [25] or vascular diseases induced by diabetes [27]. Our model corresponds rather to a major plate rupture.

4.5 TECHNICAL COMMENTS

We tried to improve the robustness of the technique both by reinforcing the low SNR expected in resting muscles and by using stable data processing. Accordingly, we used high doses of CA (1.5 times the clinical dose). However, given the detection efficiency of the DCE technique, smaller doses may be employed instead. Similarly, since the first pass phase (K_{trans}) was less stable than the late phase of the acquisition (AUCn, *Vd*, ΔS), high time resolution and precautions regarding the arterial peak concentration (double bolus) do not seem critical either. This suggests that the technique can be used under simplified acquisition conditions. Statistical tests performed on whole limbs (TOT) on non-normalized AUCs still performed well. This is encouraging for studies for which AIFs are not measurable. However, the moderate correlation between AUC and AUCn suggested that the lack of normalization may be more problematic for more flexible experimental settings. The AUCn-180 results suggest that the duration of the DCE sequence could be substantially reduced compared to our sequence. However, the strong correlation of AUCn with ΔS and some instabilities of AUCn-

180 and K_{trans} suggested that periods of a few minutes should be considered rather than 180s to reach a quasi-steady state and improve statistical power.

AUCn was particularly robust to noise. It minimized the impact of moderate SNR on parametric maps. The comparison with the simple TK compartmental analysis tool demonstrated that AUCn maps were equivalent with *Vd* maps. In addition, it indicates that the TK model does not provide additional information versus AUCn through K_{trans}, which is otherwise particularly unstable in ischemic tissues. By extension this result suggests that the level of information in the data is too limited to use any more complex model and then extract reliable quantitative physiological parameters.

The outlier detection based on the contralateral population analysis resulted in easy-to-interpret three level perfusion maps (hypo/iso/hyper). In our biological model, our population of reference was not exactly a control, but rather contralateral muscles. The extent of contralateral inflammation has not been expected. The ability of the DCE to discriminate embolized and non-embolized but moderately inflamed muscles is encouraging, because this discrimination was more challenging than versus healthy muscles and it makes sense in diagnostic terms. The search for outliers is part of statistical learning techniques [30]. The advantage of this approach is that it does not make assumptions about the nature of the anomaly to be searched for.

4.6 SCOPE AND LIMITS

The first limitation of our study was the moderate number of rabbits included in the analysis. However, the detection efficiency achieved with this small population clearly demonstrated the value of measuring perfusion heterogeneity. Furthermore, apart from the above-mentioned limits, the histologic analysis allowed us to confirm the severity of the biological

model. But an individual correlation between MRI and more elaborate staining, including CD31, would have been of great interest to validate AUCn maps physiologically. However, in a heterogeneous context like the one highlighted here, validation by histology requires a dedicated acquisition protocol. This topic is beyond the scope of this study, the purpose of which was the diagnostic efficiency of the DCE. In this study we showed that it was possible to efficiently detect embolized muscles at 7 days using DCE. However, this was demonstrated only for a massive embolization. The quality of the parametric maps suggests that detection remains possible for more local pathologies, but our study does not show to what extent the technique remains efficient when the lesions decrease in size. In addition, the sequence used on animals (multi-2D sequence) did not correspond to the clinical practice. In clinical practice, acceleration techniques are available and 3D sequences with lower temporal resolution are used. As high temporal resolution does not seem to be useful, the use of a 3D sequence seems particularly advantageous to fully explore limb perfusion. In addition, the low TR of 3D sequences tends to reduce the effects of non-linearity between MRI signal and CA concentration. However, if signal saturation effects appear, and if the acquisition center has reliable signal correction tools, such as by using T1 mapping, non-linearity could be corrected before AUCn processing.

5 CONCLUSION

This preliminary study indicated that conventional DCE results found at rest can be corrected efficiently by improved analytical methods. The study confirmed the interest of the DCE-MRI to identify muscle defects involved in arterial embolization in a rabbit model. This technique, including an analysis of heterogeneity and an outlier-detection mapping, enabled the detection of perfusion defects induced by embolization and a clear delineation between

hypo- and hyper-perfused regions, corresponding to ischemia and viable compensation regions, respectively. The previous negative results at rest are explained by the presence of local hyperemia that was not conventionally sought. The simplicity of the *AUCn* processing, the quality of the resulted *AUCn* maps, and the numerical efficiency of the detection of the perfusion defects at rest, suggested a possible translation in clinical studies, even in centers with moderate DCE experience.

REFERENCES

1. Norgren L, Hiatt WR, Dormandy JA, Nehler MR, Harris KA, Fowkes FGR. Inter-Society Consensus for the Management of Peripheral Arterial Disease (TASC II). *Journal of Vascular Surgery*. 2007;45(1):S5-S67. doi:10.1016/j.jvs.2006.12.037

2. Dua A, Lee CJ. Epidemiology of Peripheral Arterial Disease and Critical Limb Ischemia. *Techniques in Vascular and Interventional Radiology*. 2016;19(2):91-95. doi:10.1053/j.tvir.2016.04.001

3. Biancari F. Meta-analysis of the prevalence, incidence and natural history of critical limb ischemia. *J Cardiovasc Surg (Torino)*. 2013;54(6):663-669.

4. Faglia E, Clerici G, Caminiti M, et al. Mortality after major amputation in diabetic patients with critical limb ischemia who did and did not undergo previous peripheral revascularization. *Journal of Diabetes and its Complications*. 2010;24(4):265-269. doi:10.1016/j.jdiacomp.2009.02.004

5. Farber A, Eberhardt RT. The Current State of Critical Limb Ischemia: A Systematic Review. *JAMA Surgery*. 2016;151(11):1070-1077. doi:10.1001/jamasurg.2016.2018

6. Clair D, Shah S, Weber J. Current State of Diagnosis and Management of Critical Limb Ischemia. *Curr Cardiol Rep*. 2012;14(2):160-170. doi:10.1007/s11886-012-0251-4

7. Chao CYL, Cheing GLY. Microvascular dysfunction in diabetic foot disease and ulceration. *Diabetes Metab Res Rev*. 2009;25(7):604-614. doi:10.1002/dmrr.1004

8. Hur S, Jae HJ, Jang Y, et al. Quantitative Assessment of Foot Blood Flow by Using Dynamic Volume Perfusion CT Technique: A Feasibility Study. *Radiology*. 2016;279(1):195-206. doi:10.1148/radiol.2015150560

9. Aboyans V, Ho E, Denenberg JO, Ho LA, Natarajan L, Criqui MH. The association between elevated ankle systolic pressures and peripheral occlusive arterial disease in diabetic and nondiabetic subjects. *J Vasc Surg*. 2008;48(5):1197-1203. doi:10.1016/j.jvs.2008.06.005

10. Arsenault KA, Al-Otaibi A, Devereaux PJ, Thorlund K, Tittley JG, Whitlock RP. The Use of Transcutaneous Oximetry to Predict Healing Complications of Lower Limb Amputations: A Systematic Review and Meta-analysis. *European Journal of Vascular and Endovascular Surgery*. 2012;43(3):329-336. doi:10.1016/j.ejvs.2011.12.004

11. Stacy MR, Zhou W, Sinusas AJ. Radiotracer Imaging of Peripheral Vascular Disease. *J Nucl Med Technol*. 2015;43(3):185-192. doi:10.2967/jnumed.112.115105

12. Gordon Y, Partovi S, Müller-Eschner M, et al. Dynamic contrast-enhanced magnetic resonance imaging: fundamentals and application to the evaluation of the peripheral perfusion. *Cardiovascular Diagnosis and Therapy*. 2014;4(2):147-164.

13. de Bazelaire C, Calmon R, Thomassin I, et al. Accuracy of perfusion MRI with high spatial but low temporal resolution to assess invasive breast cancer response to neoadjuvant chemotherapy: a retrospective study. *BMC Cancer*. 2011;11:361. doi:10.1186/1471-2407-11-361

14. Curiel RV, Jones R, Brindle K. Magnetic resonance imaging of the idiopathic inflammatory myopathies: structural and clinical aspects. *Ann N Y Acad Sci*. 2009;1154:101-114. doi:10.1111/j.1749-6632.2009.04386.x

15. Luo. Evaluation of tissue perfusion in a rat model of hind-limb muscle ischemia using dynamic contrast-enhanced magnetic resonance imaging (vol 16, pg 277, 2002). *J Magn Reson Imaging*. 2002;16(5):620-620. doi:10.1002/jmri.10221

16. Ganesh T, Zakher E, Estrada M, Cheng HM. Assessment of microvascular dysfunction in acute limb ischemia-reperfusion injury. *J Magn Reson Imaging*. 2019;49(4):1174-1185. doi:10.1002/jmri.26308

17. Zakher E, Ganesh T, Cheng HLM. A novel MRI analysis for assessment of microvascular vasomodulation in low-perfusion skeletal muscle. *Sci Rep*. 2020;10:4705. doi:10.1038/s41598-020-61682-z

18. Del Giudice C, Ifergan G, Goudot G, et al. Evaluation of a new model of hind limb ischemia in rabbits. *J Vasc Surg*. 2018;68(3):849-857. doi:10.1016/j.jvs.2017.07.140

19. Roberts C, Buckley DL, Parker GJM. Comparison of errors associated with single- and multi-bolus injection protocols in low-temporal-resolution dynamic contrast-enhanced tracer kinetic analysis. *Magnetic Resonance in Medicine*. 2006;56(3):611-619. doi:https://doi.org/10.1002/mrm.20971

20. Versluis B, Backes WH, van Eupen MGA, et al. Magnetic Resonance Imaging in Peripheral Arterial Disease: Reproducibility of the Assessment of Morphological and Functional Vascular Status. *Investigative Radiology*. 2011;46(1):11-24. doi:10.1097/RLI.0b013e3181f2bfb8

21. Sourbron SP, Buckley DL. Classic models for dynamic contrast-enhanced MRI. *NMR in Biomedicine*. 2013;26(8):1004-1027. doi:https://doi.org/10.1002/nbm.2940

22. Shukla-Dave A, Obuchowski NA, Chenevert TL, et al. Quantitative imaging biomarkers alliance (QIBA) recommendations for improved precision of DWI and DCE-MRI

derived biomarkers in multicenter oncology trials. *Journal of Magnetic Resonance Imaging*. 2019;49(7):e101-e121. doi:10.1002/jmri.26518

23. Balvay D, Troprès I, Billet R, et al. Mapping the zonal organization of tumor perfusion and permeability in a rat glioma model by using dynamic contrast-enhanced synchrotron radiation CT. *Radiology*. 2009;250(3):692-702. doi:10.1148/radiol.2501071929

24. de Lussanet QG, van Golde JCG, Beets-Tan RGH, et al. Dynamic contrast-enhanced MRI of muscle perfusion combined with MR angiography of collateral artery growth in a femoral artery ligation model. *NMR Biomed*. 2007;20(8):717-725. doi:10.1002/nbm.1133

25. Tang GL, Chang DS, Sarkar R, Wang R, Messina LM. The effect of gradual or acute arterial occlusion on skeletal muscle blood flow, arteriogenesis, and inflammation in rat hindlimb ischemia. *Journal of Vascular Surgery*. 2005;41(2):312-320. doi:10.1016/j.jvs.2004.11.012

26. Yu J, Dardik A. A Murine Model of Hind Limb Ischemia to Study Angiogenesis and Arteriogenesis. *Methods Mol Biol*. 2018;1717:135-143. doi:10.1007/978-1-4939-7526-6_11

27. Kashiwagi Y, Nodaira M, Amitani M, Murase K, Abe K. Assessment of peripheral tissue perfusion disorder in streptozotocin-induced diabetic rats using dynamic contrast-enhanced MRI. *Magnetic Resonance Imaging*. 2012;30(2):254-260. doi:10.1016/j.mri.2011.09.018

28. Galbraith SM, Lodge MA, Taylor NJ, et al. Reproducibility of dynamic contrast-enhanced MRI in human muscle and tumours: comparison of quantitative and semi-quantitative analysis. *NMR in Biomedicine*. 2002;15(2):132-142. doi:10.1002/nbm.731

29. Adil IH, Zaman A. Outliers Detection in Skewed Distributions: Split Sample Skewness Based Boxplot. *Econ Comput Econ Cybern Stud*. 2020;54(3):279-296. doi:10.24818/18423264/54.3.20.17

30. Domingues R, Filippone M, Michiardi P, Zouaoui J. A comparative evaluation of outlier detection algorithms: Experiments and analyses. *Pattern Recognit*. 2018;74:406-421. doi:10.1016/j.patcog.2017.09.037

31. Murray AK. Laser Doppler imaging: a developing technique for application in the rheumatic diseases. *Rheumatology*. 2004;43(10):1210-1218. doi:10.1093/rheumatology/keh275

32. Castro PR, Barbosa AS, Pereira JM, et al. Cellular and Molecular Heterogeneity Associated with Vessel Formation Processes. BioMed Research International. doi:10.1155/2018/6740408

33. Cooke JP, Losordo DW. Modulating the Vascular Response to Limb Ischemia Angiogenic and Cell Therapies. *Circulation Research*. 2015;116(9):1561-1578. doi:10.1161/CIRCRESAHA.115.303565

34. Ziv K, Nevo N, Dafni H, et al. Longitudinal MRI tracking of the angiogenic response to hind limb ischemic injury in the mouse. *Magnetic Resonance in Medicine*. 2004;51(2):304-311. doi:10.1002/mrm.10687

35. Hoefer IE, van Royen N, Buschmann IR, Piek JJ, Schaper W. Time course of arteriogenesis following femoral artery occlusion in the rabbit. *Cardiovasc Res*. 2001;49(3):609-617. doi:10.1016/S0008-6363(00)00243-1

36. Shireman PK. The chemokine system in arteriogenesis and hind limb ischemia. *Journal of Vascular Surgery*. 2007;45(6):A48-A56. doi:10.1016/j.jvs.2007.02.030

37. Jiji RS, Pollak AW, Epstein FH, et al. Reproducibility of rest and exercise stress contrast-enhanced calf perfusion magnetic resonance imaging in peripheral arterial disease. *Journal of Cardiovascular Magnetic Resonance*. 2013;15(1):14. doi:10.1186/1532-429X-15-14

38. Venkatesh BA, Nauffal V, Noda C, et al. Baseline assessment and comparison of arterial anatomy, hyperemic flow, and skeletal muscle perfusion in peripheral artery disease: The Cardiovascular Cell Therapy Research Network “Patients with Intermittent Claudication Injected with ALDH Bright Cells” (CCTRN PACE) study. *Am Heart J*. 2017;183:24-34. doi:10.1016/j.ahj.2016.09.013

Table 1. *MRI parameters of T2-w, T1-w post-injection and DCE sequences*

___

Figure 1. *a T2-weighted image and anatomic segmentation of the lower limb in the transverse plane. (A) Arrowheads show muscle tear ("feather like" pattern) and stars, tendinitis. Three muscle groups were delimited in an embolized limb (red dotted line): (B) Anterior muscles in yellow (tibialis anterior, extensor digitorum longus), deep in green (flexor digitorum longus) and posterior in blue (soleus, lateral and medial gastrocnemius, plantaria).*

Figure 2. *Contrast enhancement in muscle regions for a rabbit with two opposite responses to embolization. The contralateral muscles (full lines) show homogeneous enhancements unlike embolized muscles (dashed lines). The anterior (yellow) and posterior (blue) muscle groups have no enhancement (ischemia) while the deep (green) muscle groups shows a clear increase in perfusion compared to contralateral muscles. The signal amplitude corresponds to the MRI signal intensity after baseline subtraction. Its unit is arbitrary. This is why the signal is normalized by that of the arterial input function in AUCn.*

Figure 3*. Tofts-Kety parameters* K_{trans} *and* V_d*, and normalized Area Under the curve (AUCn) on ROIs of muscle groups. (**Left in panels**) Embolized muscles. (**Right in panels**) Contralateral muscles. Colors: (**Black)** anterior muscles, (**gray**) deep muscles and (**white**) posterior muscles. Not paired Wilcoxon (Wcx) and Fisher tests (F-Test) were performed on* K_{trans}*, volume fraction of distribution (Vd), and **AUCn**. No reduction in perfusion was observed on average in the embolized muscles but the variability between embolized muscles increased significantly. Increases in variance greater than 200% were noted, as indicated below the panels (var:—%). Surprisingly, almost 90% of the* V_d *and AUCn values obtained in the embolized muscles were outside the range of values obtained in contralateral muscles. The percentage of values out of the contralateral range was noted as out:—%. AUCn is a ratio, and therefore has no unit (nu)*

Figure 4*. Features calculated on AUCn maps in embolized and contralateral sides.* ***(A)*** *central-tendency features, including average, median and mode. A difference was noted with the Wilcoxon-Test (Wcx) only for the mode.* ***(B)*** *Dispersion features, including standard deviation (SD), median absolute deviation (MAD) and the range. The dispersion increased significantly according to all these features.* ***(C)*** *Outlier features, including 5% and 95% percentiles (p5% and p95% resp.), low, high and total outlier fractions (LOF, HOF, TOF). The number of high, low and total outliers was significantly increased. Notation: ** indicates P <0.01, + indicates no overlap between Embolized and Contralateral AUCn values.*

Figure 5. *AUCn and derivative detection maps for embolized and contralateral limbs. Detection maps provided three levels of perfusion: hypo (dark), iso (gray) and hyper-perfusion (white), based on an automated outlier detection. The detection thresholds were learned in all pixels of the contralateral limbs. Both hypo and hyper perfused areas characterize embolized limbs. Perfusion maps were homogeneous on the contralateral side, except for one rabbit (star) previously excluded due to a major inflammation of the contralateral limb.*

Figure 6*. Classification of the muscle groups provided by a decision tree based on average (y) and standard deviation (x) in the muscle group maps. The embolized muscle groups were either characterized by an almost zero average AUCn (bottom) or characterized by high standard deviations of AUCn compared to the contralateral muscles (right). AUCn is a ratio, it has no unit*

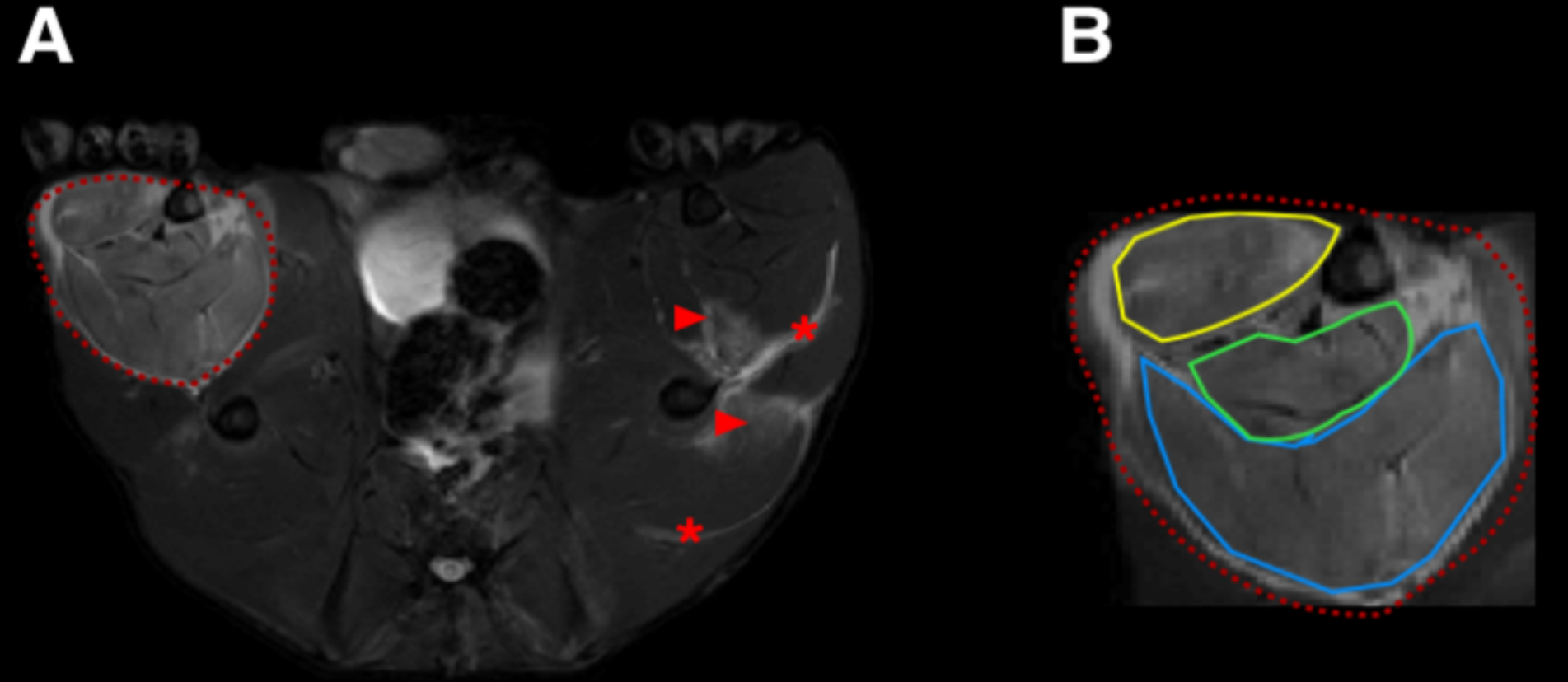
A
B


Contrast Enhancements in muscle regions (R 148)
POST CONT
POST EMB
DEEP CONT
DEEP EMB
ANT CONT
ANT EMB
3000
2000
1000
0
-500
0
200
400
600
750
Time (s)

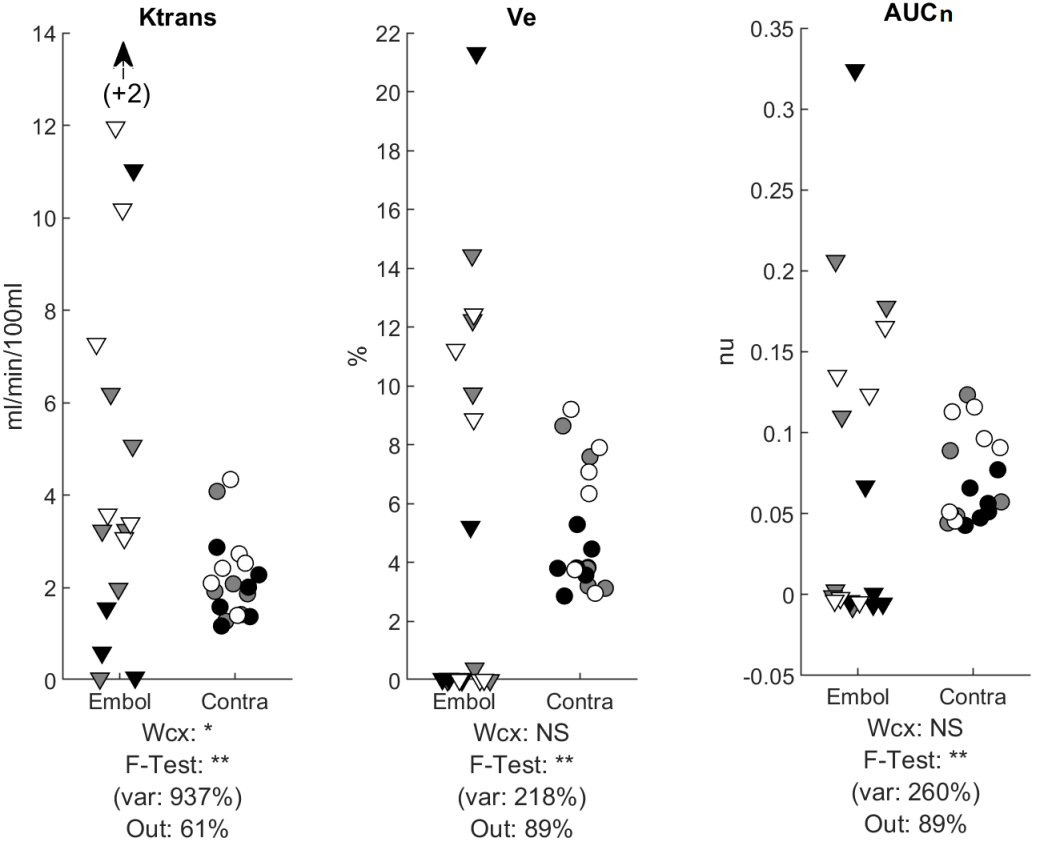
Ktrans
(+2)
ml/min/100ml
14
12
10
8
6
4
2
0
Embol
Contra
Wcx: *
F-Test: **
(var: 937%)
Out: 61%
Ve
%
22
20
18
16
14
12
10
8
6
4
2
0
Embol
Contra
Wcx: NS
F-Test: **
(var: 218%)
Out: 89%
AUCn
nu
0.35
0.3
0.25
0.2
0.15
0.1
0.05
0
-0.05
Embol
Contra
Wcx: NS
F-Test: **
(var: 260%)
Out: 89%

A

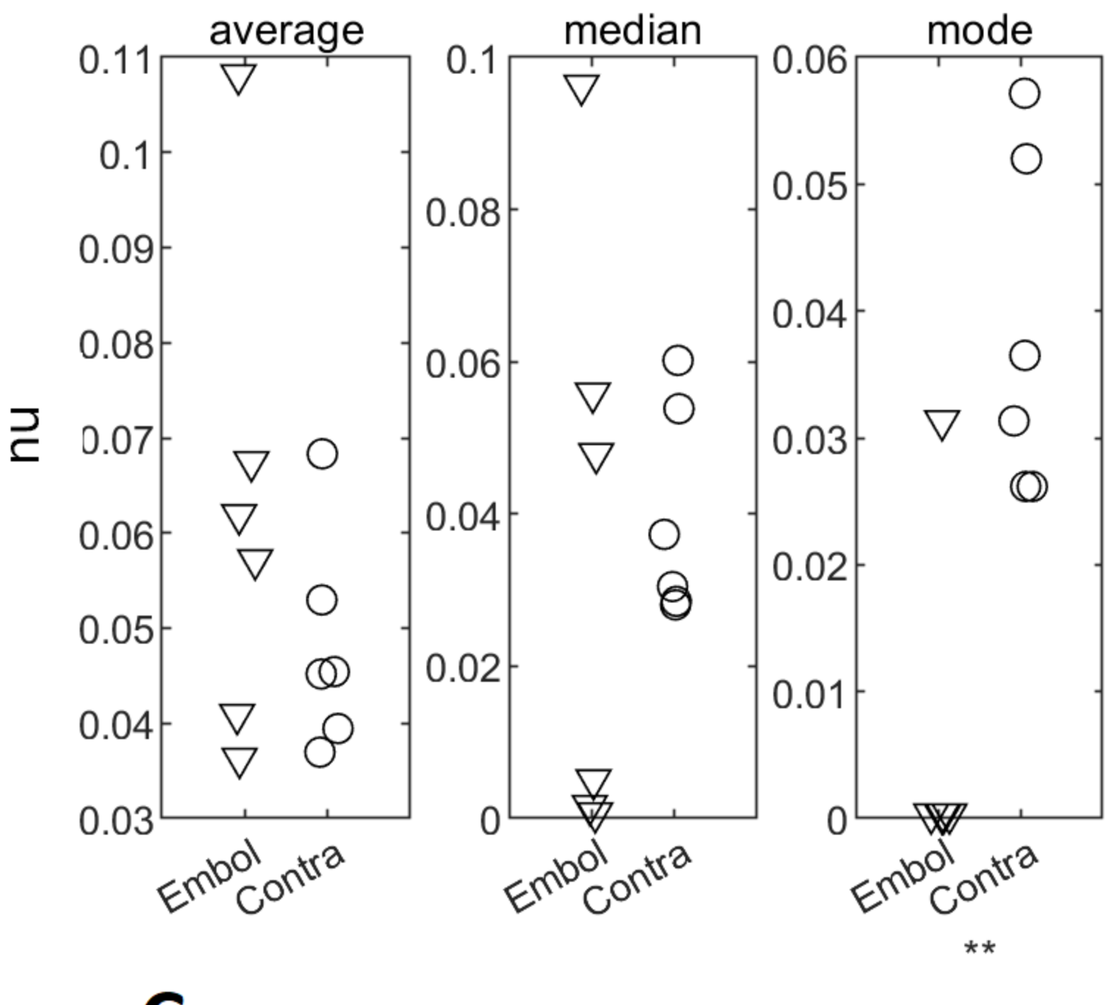
average
median
mode
nu
0.11
0.1
0.09
0.08
0.07
0.06
0.05
0.04
0.03
0.1
0.08
0.06
0.04
0.02
0
0.06
0.05
0.04
0.03
0.02
0.01
0
Embol
Contra
**

B

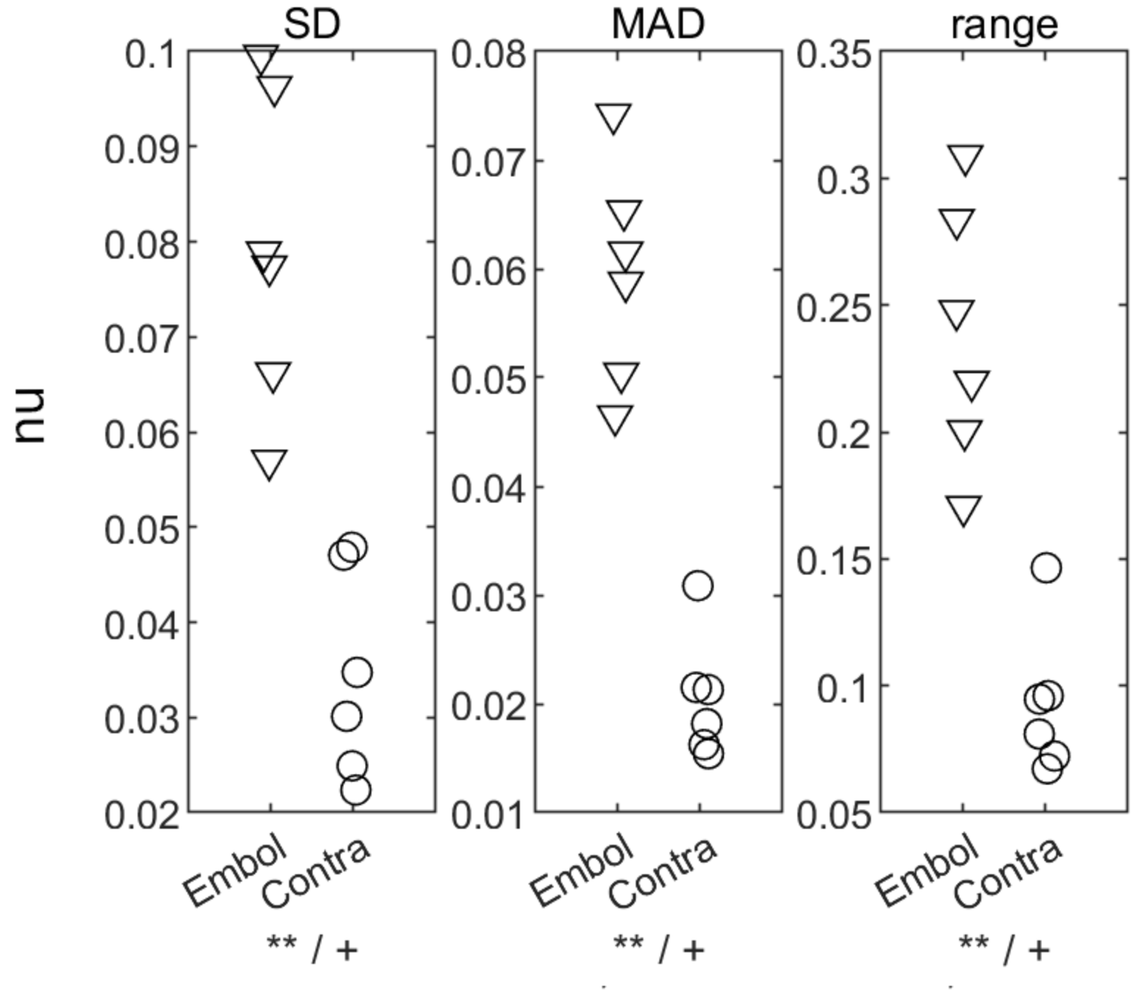
SD
MAD
range
nu
0.1
0.09
0.08
0.07
0.06
0.05
0.04
0.03
0.02
0.08
0.07
0.06
0.05
0.04
0.03
0.02
0.01
0.35
0.3
0.25
0.2
0.15
0.1
0.05
Embol
Contra
** / +

C

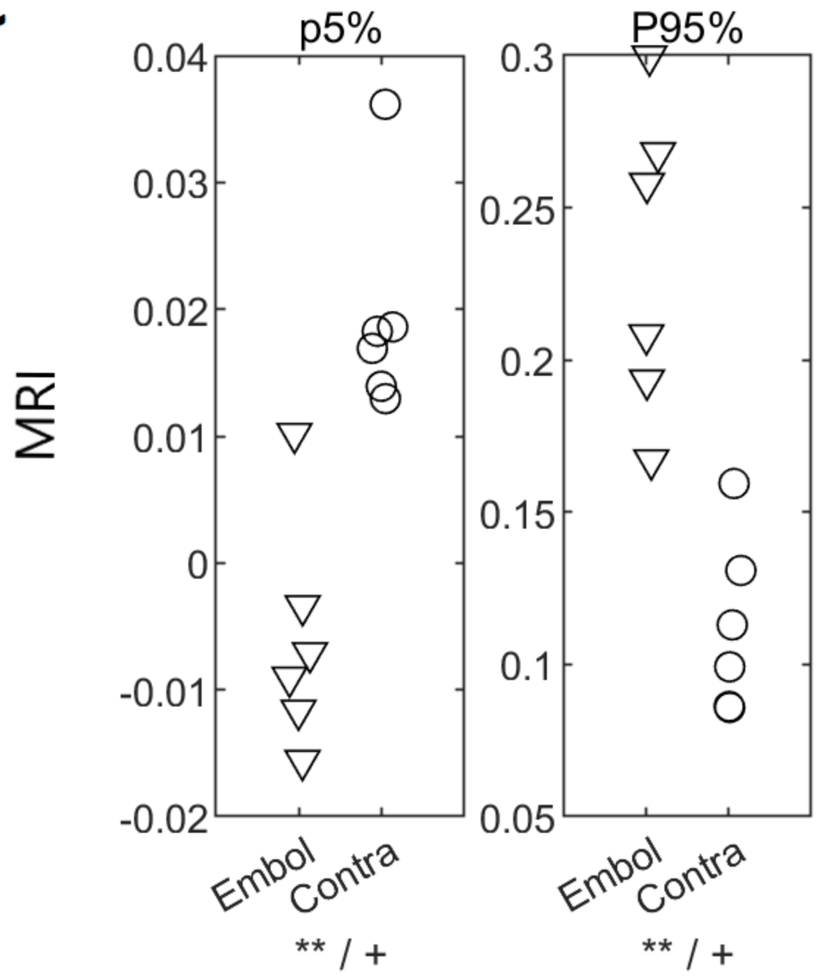
p5%
P95%
MRI
0.04
0.03
0.02
0.01
0
-0.01
-0.02
0.3
0.25
0.2
0.15
0.1
0.05
Embol
Contra
** / +

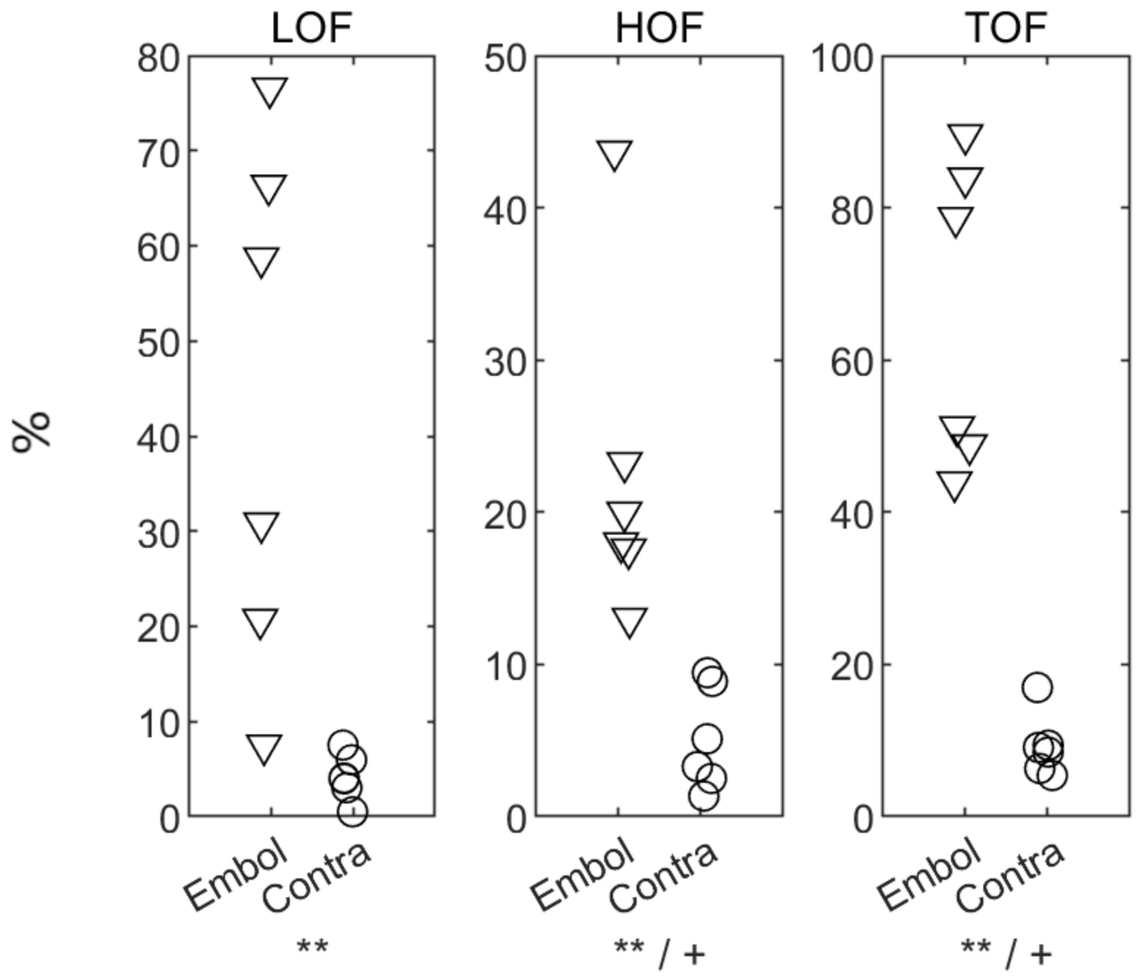
LOF
HOF
TOF
%
80
70
60
50
40
30
20
10
0
50
40
30
20
10
0
100
80
60
40
20
0
Embol
Contra
**
** / +

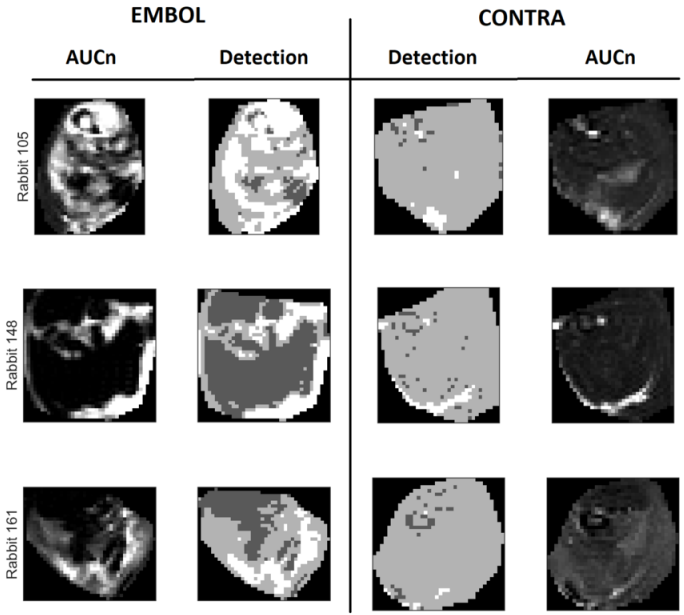
EMBOL
CONTRA
AUCn
Detection
Detection
AUCn
Rabbit 105
Rabbit 148
Rabbit 161

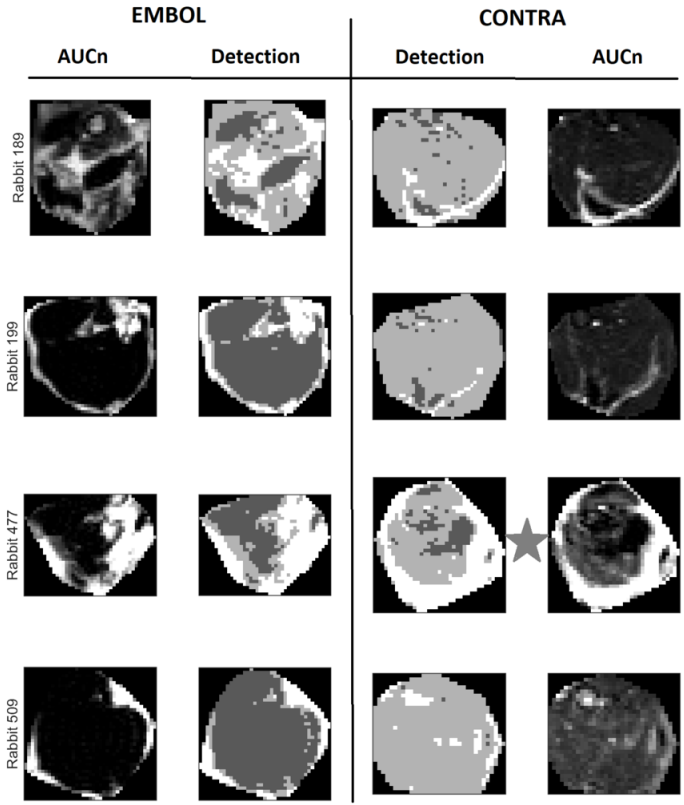
EMBOL
CONTRA
AUCn
Detection
Detection
AUCn
Rabbit 189
Rabbit 199
Rabbit 477
Rabbit 509

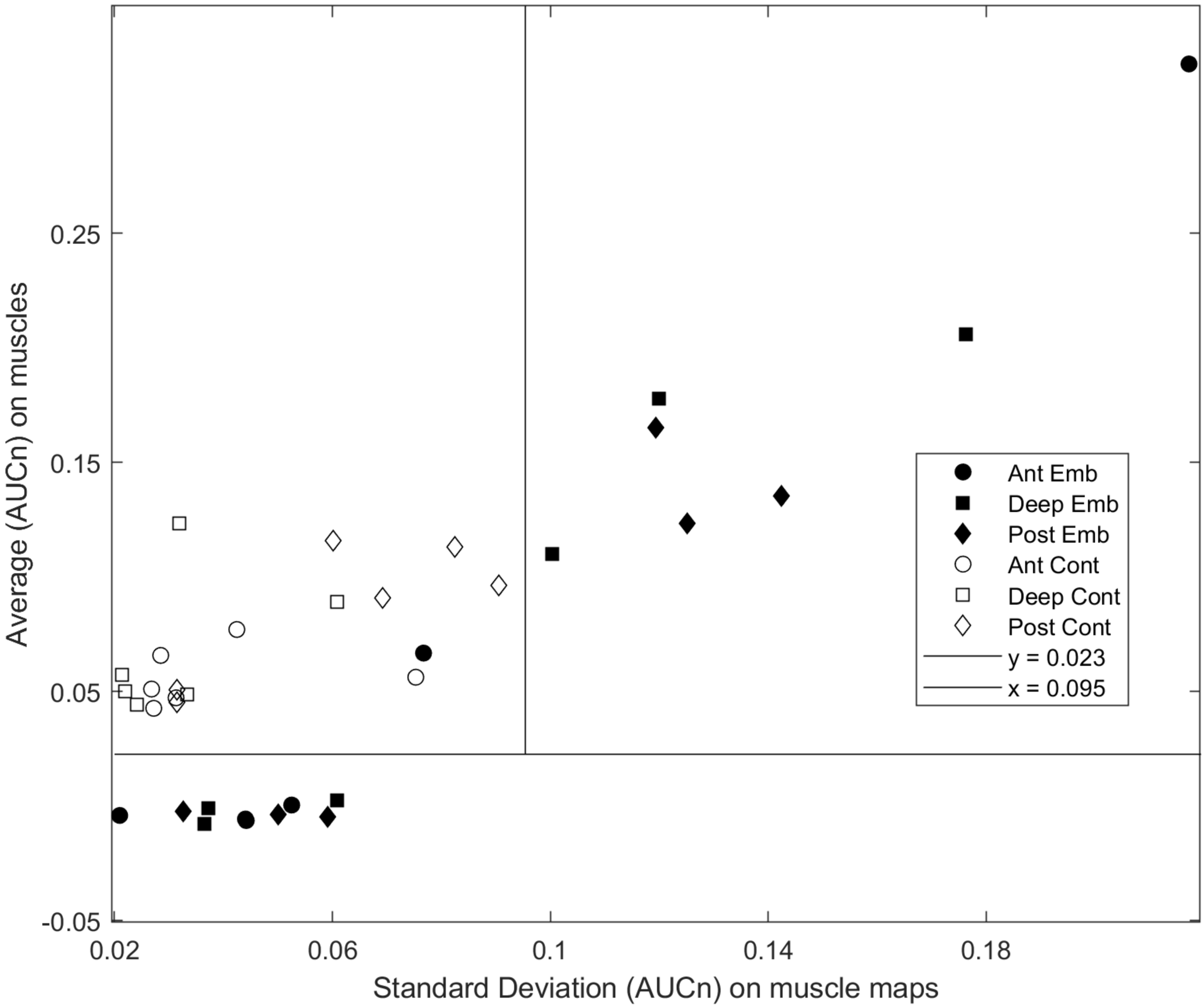
0.25
0.15
0.05
-0.05
0.02
0.06
0.1
0.14
0.18
Average (AUCn) on muscles
Standard Deviation (AUCn) on muscle maps
Ant Emb
Deep Emb
Post Emb
Ant Cont
Deep Cont
Post Cont
y = 0.023
x = 0.095

Table 1. MRI parameters of T2-w, T1-w post-injection and DCE sequences

Sequences	TR (ms)	TE (ms)	Flip angle	FOV (cm)	Spatial Resolution (micron)	Slice thickness (mm)	Number of axial slices	Number of average	Acquisition time
2D T2-w turbo RARE	4000	50	SE	20 × 15	781 × 586	5	13	3	6min24s
2D FLASH DCE	25	3	90°	20 × 15	1176 × 1172	5	3	1	12min7s
2D T1-w turbo RARE Post injection	1000	12	SE	20 × 15	781 × 586	5	13	6	4min48s

TR: Repetition Time; TE: Echo Time; FOV: Field Of View; RARE: Rapid Acquisition with Refocused Echoes; FLASH: Fast Low Angle Shot